How to cite: *Angew. Chem. Int. Ed.* **2021**, *60*, 1458–1464
International Edition: doi.org/10.1002/anie.202011858
German Edition: doi.org/10.1002/ange.202011858

Surface Chemistry

Azo bond formation on metal surfaces

Xiangzhi Meng[+], Henning Klaasen[+], Lena Viergutz, Bertram Schulze Lammers, Melanie C. Witteler, Harry Mönig, Saeed Amirjalayer, Lacheng Liu, Johannes Neugebauer, Hong-Ying Gao, Armido Studer,* and Harald Fuchs**

Abstract: *The formation of azo compounds via redox cross-coupling of nitroarenes and arylamines, challenging in solution phase chemistry, is achieved by on-surface chemistry. Reaction products are analyzed with a cryogenic scanning tunneling microscope (STM) and X-ray photoelectron spectroscopy (XPS). By using well-designed precursors containing both an amino and a nitro functionality, azo polymers are prepared on surface via highly efficient nitro-amino cross-coupling. Experiments conducted on other substrates and surface orientations reveal that the metal surface has a significant effect on the reaction efficiency. The reaction was further found to proceed from partially oxidized/reduced precursors in dimerization reactions, shedding light on the mechanism that was studied by DFT calculations.*

Introduction

During the last decade, on-surface chemistry has attracted extensive attention as a bottom-up strategy for the synthesis of materials with interesting properties and functions. Various organic reactions have been successfully realized on metal surfaces[1–4] and most of them aim for carbon–carbon bond formation. Only a few carbon–nitrogen and nitrogen–nitrogen bond forming processes have been reported, such as imine,[5–7] imide,[8] azo group formation[9–11] and azide–alkyne cycloaddition.[12,13] Among these N-based functional groups, the azo group shows valuable properties in photo switching.[14–16] In solution phase chemistry, azo compounds are obtained through an azo coupling using diazonium salts, but the cross-coupling of nitro and amino compounds remains challenging. Herein, on-surface azo formation by nitroarene–arylamine redox cross-coupling (path **1** in Scheme 1a) is successfully realized on the Ag(111) surface under ultrahigh vacuum (UHV) conditions. On-surface azo formation via

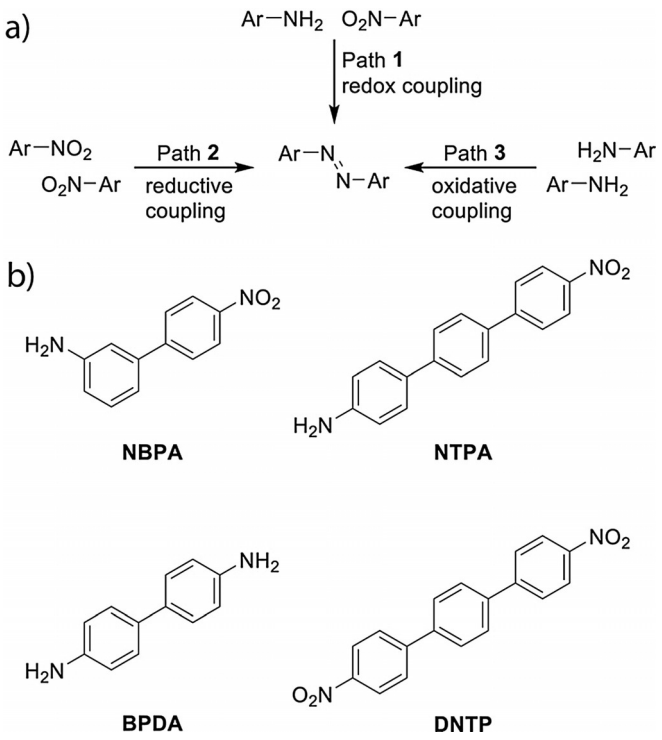

Scheme 1. a) Investigated coupling pathways and b) bifunctional monomers towards on-surface azo group formation.

[*] Dr. X. Meng,[+] B. Schulze Lammers, Dr. H. Mönig, Dr. S. Amirjalayer, L. Liu, Dr. H. Y. Gao, Prof. H. Fuchs
Physikalisches Institut
Westfälische Wilhelms-Universität Münster
Wilhelm-Klemm-Strasse 10, 48149 Münster (Germany)
and
Center for Nanotechnology
Heisenbergstrasse 11, 48149 Münster (Germany)
E-mail: gaohongying@tju.edu.cn
fuchsh@uni-muenster.de

Dr. H. Klaasen,[+] L. Viergutz, M. C. Witteler, Prof. J. Neugebauer, Prof. A. Studer
Organisch-Chemisches Institut
Westfälische Wilhelms-Universität Münster
Corrensstrasse 40, 48149 Münster (Germany)
E-mail: studer@uni-muenster.de

Dr. X. Meng,[+] Prof. A. Studer, Prof. H. Fuchs
Institution Center for Soft Nanoscience
Busso-Peus-Strasse 10, 48149 Münster (Germany)

M. C. Witteler, Dr. S. Amirjalayer, Prof. J. Neugebauer
Center for Multiscale Theory and Computation
Westfälische Wilhelms-Universität
Corrensstrasse 40, 48149 Münster (Germany)

Dr. H. Y. Gao
School of Chemical Engineering and Technology
Tianjin University
Tianjin 300072 (China)

[+] Theses authors contributed equally to this work.

Supporting information and the ORCID identification number(s) for the author(s) of this article can be found under: https://doi.org/10.1002/anie.202011858.

reductive nitroarene or oxidative arylamine homocoupling (paths **2** and **3** in Scheme 1a) shows poor efficiency. Low-temperature scanning tunneling microscopy (LT-STM) and X-ray photoelectron spectroscopy (XPS) were applied for product analysis. The chemical structures of organic precursors used are depicted in Scheme 1b (for their synthesis, see the Supporting Information, SI). By using well-designed precursors, azo polymers and alternating azo oligomers are accessible on-surface. In addition, the effect of the metal surface on the azo formation is investigated.

Results and Discussion

To distinguish the three possible coupling reactions (paths **1**–**3** in Scheme 1a), the unsymmetrical bifunctional 4′-nitrobiphenyl-3-amine (**NBPA**) was studied on the Ag(111) surface (Figure 1). After adsorption on Ag(111) kept at room temperature (RT), **NBPA** assembled into a well-ordered monolayer (Figure 1a). The self-assembly exhibits a hexagonal honeycomb motif composed of hexamer units, in which H-bonding is assumed between the nitro and amino groups.[17] After annealing (393 K), azo groups were formed (as further supported by XPS analysis, see below) resulting in cyclic oligomers (Figure 1c) and long chains (Figure 1d). According to the STM images, most of the azo groups were formed via nitro–amino coupling (black arrows in Figure 1c,d), as estimated by the angle at the connection points between the monomeric units. Few azo groups (ca. 15%) were formed through nitro–nitro homocoupling (white arrows in Figure 1b,d) and azo groups resulting from amino–amino coupling were rarely observed. For **NBPA**, the reaction efficiency in Scheme 1a could be ranked as path **1** ≫ path **2** > path **3**. In line with this finding, reductive homocoupling of 4,4″-dinitro-*p*-terphenyl (**DNTP**), a monomeric precursor designed to follow reaction pathway **2**, showed low efficiency on Ag(111) (Figure S1) and only short azo chains were obtained. To further validate the selectivity, monofunctional aromatic precursors were tested in cross-dimerization experiments (see SI). In agreement with the reactivity trend observed for **NBPA**, nitro–amino and nitro–nitro couplings were noted, whereas products derived from arylamine homocouplings following path **3** were rarely identified (Figure S2–S5). In case of the attempted aniline homocouplings, we identified amides coordinating to surface adatoms. Importantly, it was found that electron-withdrawing groups attached to the aniline reduce the amount of these adatoms. We assume that amine metalation suppresses oxidative homocoupling. On the other hand, the adatoms might lead to a more reactive substrate and be beneficial for side reactions such as reductive homocoupling of nitro groups or branching. Further, it was found that rigid compounds engage in these cross-couplings more efficiently. Monomers with fixed conformation and planar structure showed a better cross-coupling selectivity (Figure S3) and the statistical analysis revealed that **NBPA**, substituted with an electron withdrawing group and low degree of conformational flexibility, afforded the highest tendency toward the redox coupling product (Figure S6). Homo-dimerization of anilines following path **3** was rarely observed without the presence of the nitro functionality in accordance with previously reported studies[18,19] (Figure S7).

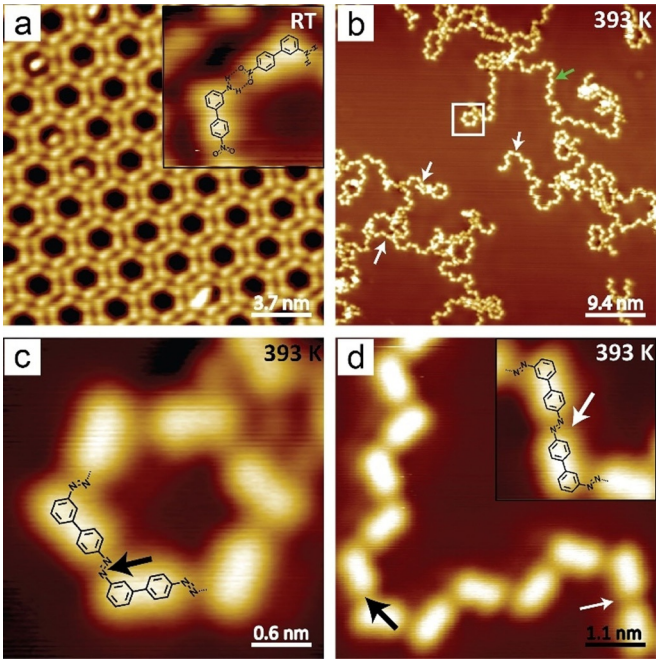

Figure 1. Azo formation on Ag(111) surface. a) STM image of **NBPA** self-assembled on Ag(111) surface after deposition at RT. Inset: zoomed-in STM image of (a). b–d) STM images after annealing the sample at 393 K for 30 min. Black arrow: azo groups formed by nitro–amino coupling. Green arrow: azo chain. Inset in (d): zoomed-in image of azo group formed by nitro–nitro coupling (white arrows). Set point: a) and inset: $U=-1.2$ V, $I=80$ pA. b–d) $U=-1.4$ V, $I=70$ pA. Size of inset in (a): 2.0×2.0 nm^2, (d): 2.3×2.3 nm^2.

To achieve long azo polymer chains and guided by the identified reactivity trend, the linear 4′-nitro-*p*-terphenyl-4-amine (**NTPA**) bearing an amino as well as a nitro functionality was prepared. The stability of **NTPA** during evaporation was confirmed with in situ mass spectrometry. Upon adsorption on the Ag(111) surface at RT, **NTPA** molecules assembled into regular sieve structures (Figure 2a,b). H-bonds are assumed to connect neighboring compounds. Resulting from the substrate symmetry, the neighboring **NTPA** molecules are not perfectly perpendicular to each other within the assembly. After annealing at 440 K for 30 min, terphenyl polymers linked by azo bonds were formed (Figure 2c). The high-resolution STM image showed that azo groups were formed with *trans*-geometry (Figure 2d). The distance between the centers of the nearest terphenyl groups is 1.51 ± 0.03 nm, which agrees with a theoretical model (Figure S8) and an ex situ prepared model azo compound that further exhibits a similar STM topography (Figure S9). Tip manipulations confirmed the covalent bonding between the polymer units (Figure S10).

Next, we tested the effect of the substrate on the reaction outcome and **NTPA** was investigated on various surfaces. For comparison, STM results recorded after annealing at 440 K are shown in Figure 3. Images showing the self-assembled structure of **NTPA** after deposition and the reaction products at other temperatures are presented in the SI (Figure S11).

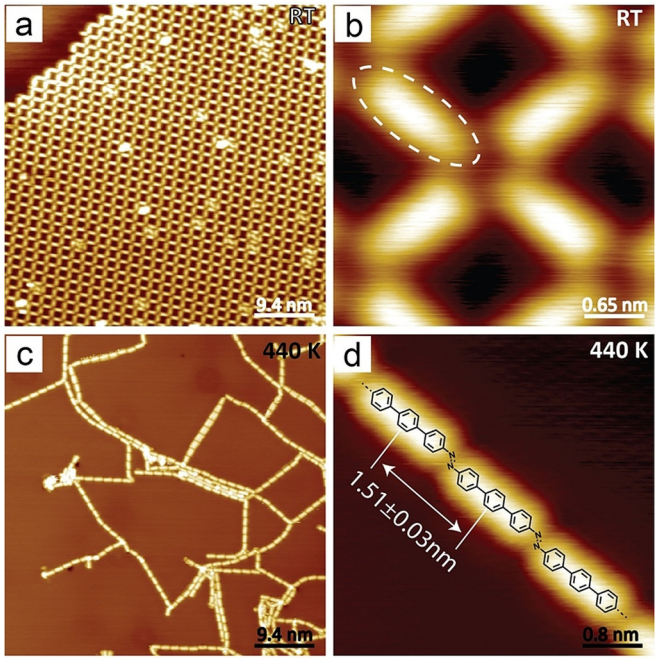

Figure 2. Synthesis of linear azo polymers on Ag(111). a) STM image of **NTPA** assembly. b) Zoomed-in STM image of (a). c) STM image of polymers obtained after annealing the sample at 440 K for 30 min. d) Zoomed-in image of the polymer. Set point: a) $U=-2$ V, $I=50$ pA; b) $U=-1$ V, $I=50$ pA; c,d) $U=-1$ V, $I=70$ pA.

On Ag(110), polymers with a similar contrast and length of the recurring motif as observed on Ag(111) were obtained after annealing at 440 K (Figure 3a,b). They tend to align along the [1$\bar{1}$0] direction of the surface, but multiple defects (green arrows in Figure 3b) were noted at the azo linkers. On Au(111), **NTPA** self-assembled in long 1D chains along the reconstructed herringbones after deposition (Figure S11e). Coupling did not occur at 440 K and the self-assembled structure remained (Figure 3c,d). The distance between the recurring motif in the chain is 1.71 ± 0.03 nm, clearly indicating linkage via H-bonding. Au(110) was more reactive and deposition of **NTPA** caused the thermodynamically unstable (1×3) reconstruction of Au(110) (Figure S11j). Annealing at 440 K led to a more pronounced formation of the (1×3) reconstruction as well as to polymerization of **NTPA** inside the (1×3) channels (Figure 3e,f). Some depressions (green arrow in Figure 3f) were observed on the polymers, which were ascribed to the missing atoms underneath. A similar phenomenon was also noted on Ag(110) (Figure S11d). The distance between two recurring moieties indicates the same outcome as found on Ag(111). Overall, the (110) surfaces provide a distinct confinement for the products, which were observed with higher order than on the (111) surfaces. Finally, reactivity of **NTPA** was studied on Cu(111). Instead of the azo formation, activation of N–H, N–O, and C–H bonds occurred. After deposition and at different annealing temperatures, clusters and short chains connected via coordination bonds (Figure 3g,h, Figure S11m–p) were the main products, in agreement with previously described dehydrogenation of aniline derivatives on Cu(111).[18,19] Overall, our experiments indicate that the azo formation reaction is highly influenced by the metal type as well as the surface structure.

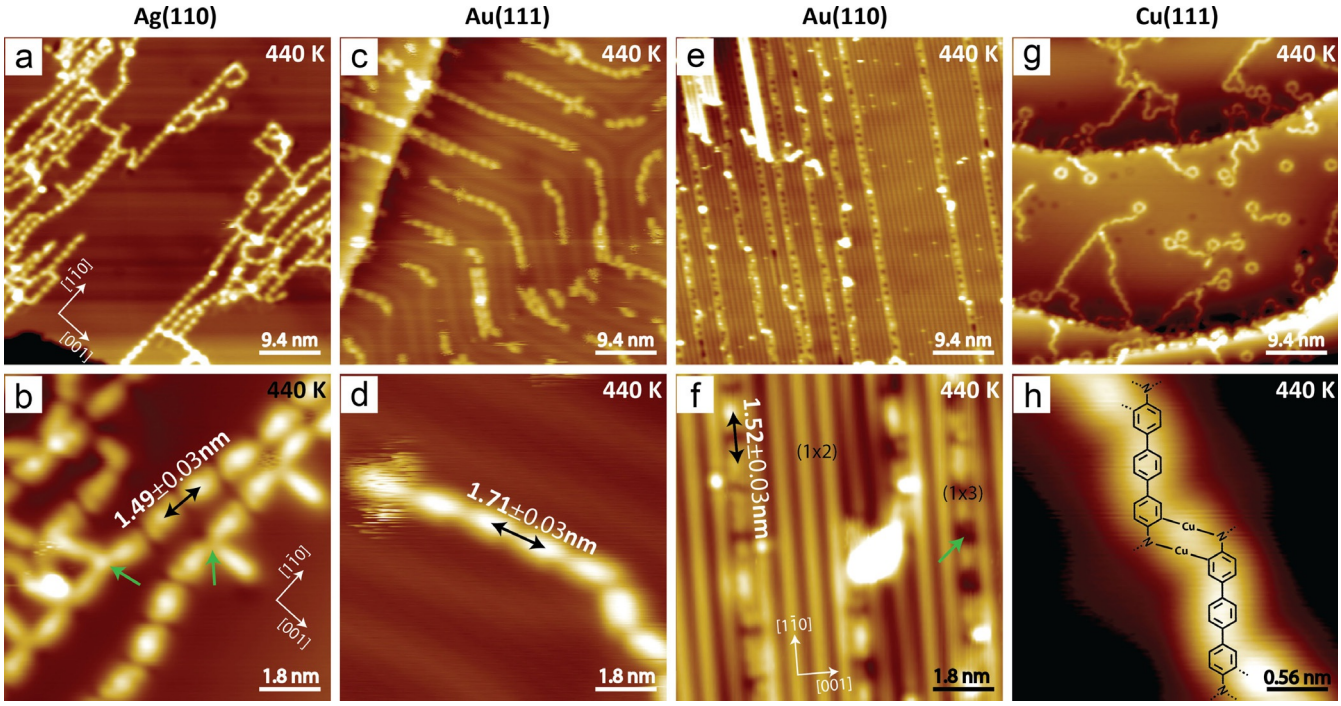

Figure 3. **NTPA** at different surfaces. a,b) STM images recorded after annealing a sub-monolayer of **NTPA** on Ag(110) at 440 K. c,d) STM images recorded after annealing a sub-monolayer of **NTPA** on Au(111) at 440 K. e,f) STM images recorded after annealing a sub-monolayer of **NTPA** on Au(110)at 440 K. g,h) STM images recorded after annealing a sub-monolayer of **NTPA** on Cu(111) at 440 K. Set points: a) $U=-1.5$ V, $I=160$ pA; b) $U=-0.2$ V, $I=370$ pA; c,d) $U=-1.1$ V, $I=47$ pA; e,f) $U=-1.3$ V, $I=130$ pA; g) $U=-0.85$ V, $I=400$ pA; h) $U=-0.14$ V, $I=570$ pA.

Attempting alternating copolymerization, **DNTP** and biphenyl-4,4′-diamine (**BPDA**) were co-adsorbed on Ag(111) (Figure 4). After deposition, ordered and disordered phases were observed, denoted by black dashed rectangle and white dashed ellipse in Figure 4a. Consistent with previous works,[18,19] the **BPDA**s were found connected by adatoms (Figure 4b,c, also see Figure S7). In the disordered phases, azo-connected oligomers were already formed at RT (white and blue arrow in Figure 4c), as also found for other monomers, usually after long-time annealing (Figure S12 and S13). Annealing (343 K) improved reaction efficiency (Figure 4d) and alternating azo chains with up to five units were identified (Figure 4e,f). A strictly alternating polymerization was difficult, as the nitro–nitro coupling of **DNTP** would introduce defects. Furthermore, **BPDA** could easily desorb from the surface at high temperature, perturbing the 1:1 stoichiometry of the two reaction partners. To achieve longer alternating polymers, strategies of surface confinement and specially designed precursors need to be considered.

To understand the chemical states, XPS experiments were conducted. The spectra recorded were analyzed using a commercial processing software (*CasaXPS*). Figure 5 shows the N 1s spectra recorded on **NTPA** samples prepared at different conditions. In the region of N 1s, the clean silver surface shows a strong background. The spectrum of the clean surface was fitted by two optimized components (not shown), whose peak positions and full width at half maxima were used to reckon the surface contribution in the analysis of the spectra on other samples. Since the coupling between nitro and amino groups can be performed at RT (Figure S12 and S13), a monolayer was deposited onto Ag(111) at 170 K to avoid a partial reaction during the XPS measurement. In the XP spectrum, a peak at a binding energy of 399.6 eV was observed and could be assigned to the amino groups.[20–22] Unfortunately, even under these conditions the nitro group could not be observed in the spectrum. After annealing at 390 K, the amino peak vanished and two new peaks were observed at 400.1 and 397.7 eV. In consistency with the STM results, the peak at 400.1 eV indicates the formation of azo groups.[23–25]

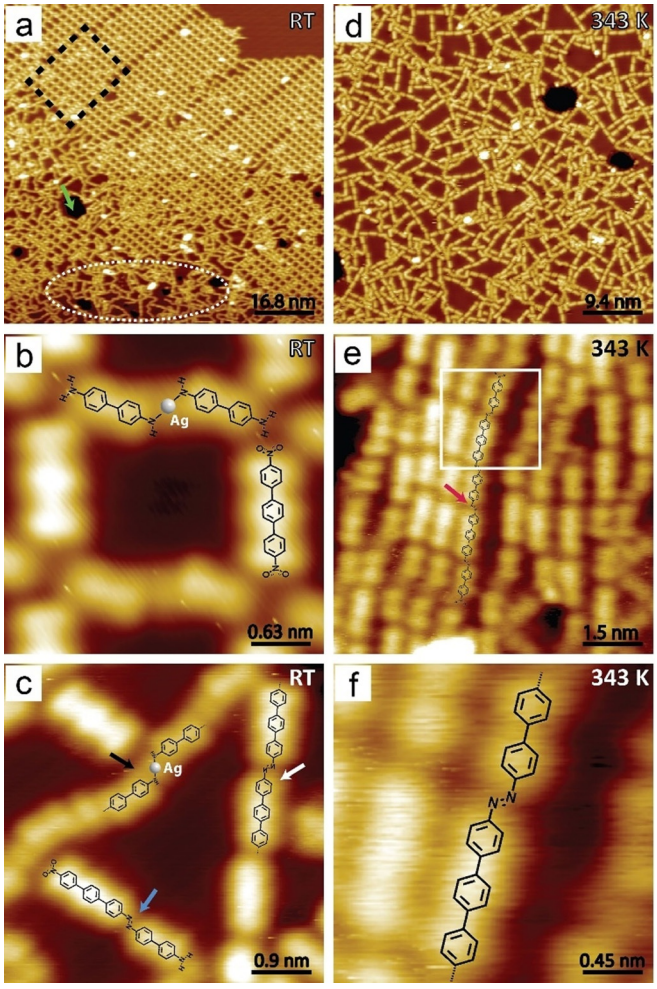

Figure 4. Towards alternating polymers on Ag(111) surface. a–c) Co-adsorption of **DNTP** and **BPDA**. a) Overview image with ordered (black rectangle) and disordered (white ellipse) structures. b) Zoomed-in ordered assembly. c) Zoomed-in disordered phase. Blue arrows: azo bond formed by nitro and amino. White arrow: terphenyl chains. Black arrow: **BPDA** chains via N–Ag–N bonds. d–f) STM images recorded after annealing at 343 K for 30 min. d) Overview image with surface hollows. e) Zoomed-in image of alternating chains. Red arrow: azo bonds. f) High resolution image of azo-linkage. Set point: a,b) $U=-1.7$ V, $I=50$ pA; c) $U=-1.7$ V, $I=60$ pA; d) $U=-1$ V, $I=50$ pA; e,f) $U=-1.3$ V, $I=45$ pA.

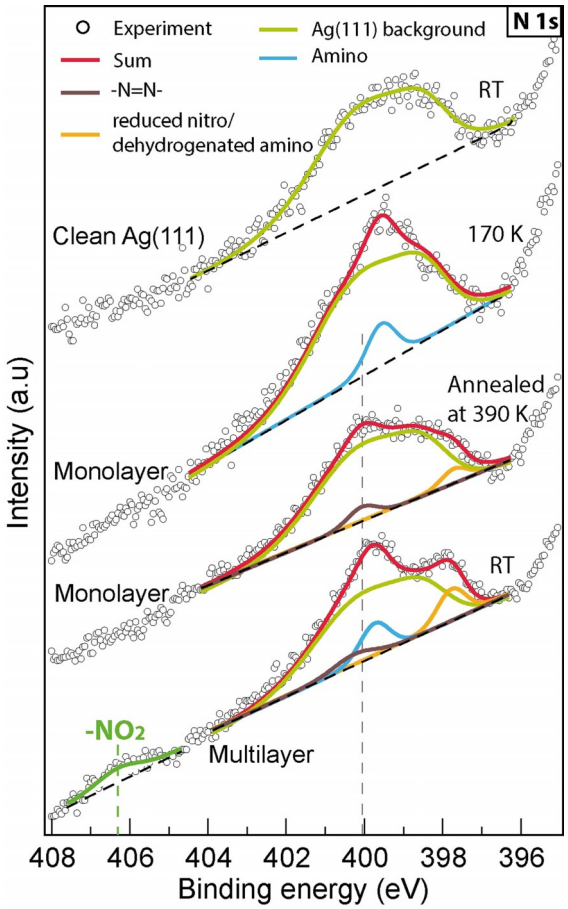

Figure 5. N 1s XP spectra recorded on a clean Ag(111) surface, NTPA monolayer adsorbed on cold Ag(111) (170 K), NTPA monolayer annealed at 390 K for 30 min, and multilayers deposited onto Ag(111) held at RT. Dashed line: azo peak.

The N 1s peaks observed on Ag(111) agree well with those of powders and reported data (Table S1). The peak at 397.7 eV is ascribed to deoxygenated nitro[26] and the dehydrogenated amino groups,[7,27,28] before azo group formation. On the multilayer sample, the N 1s peak arising from the nitro groups is observed at 406 eV.[21,29,30] The absence of the peak of nitro groups in the monolayer samples could result from the strong background as well as the easy reduction of nitro groups on the silver surface (O 1s spectra in Figure S14). The signals of intact nitro and amine groups in a monolayer of **NTPA** were only observed on the Au(111) surface (Figure S14), revealing the very low activity of these functional groups in line with their poor reaction efficiency found in STM experiments. The XP spectra concede a possible mechanistic model in which the nitro groups are deoxygenated and reduced stepwise, while the amino groups are partially oxidized and metalated. This causes the net comproportionation before azo formation. We therefore assumed that arylhydroxylamines, as a result of the weak N–O bond, should easily be metalated like amines and thus lead to reactive intermediates of the sequence. Indeed, by using *N*-(naphthalene-1-yl)hydroxylamine as starting material, dimerization towards 1,1′-azonaphthalene at 383 K was achieved at Ag(111) (Figure S15), in line with our mechanistic model as discussed below. Furthermore, nitrosoarenes could either be intermediates or act as precursors for intermediates of our reaction sequence. To validate our assumption of stepwise reduction of the nitro group we tested *p*-decyloxynitrosobenzene on Ag(111) and found a clean dimerization at 420 K (Figure S16).

With these mechanistic indications in hand, we wanted to gain further insights into the reaction mechanism. Coupling of aniline and nitrobenzene on Ag(111) to form *trans*-azobenzene was studied as a model reaction using DFT calculations. A four-layered slab model with a calculated lattice constant of 4.07 Å was used to sample the Ag(111) surface. The calculations were performed with the PBE functional,[31,32] the wave functions were expanded in a plane-wave basis with an energy cut off of 500 eV and a $3\times3\times1$ k-point grid was used to sample the Brillouin Zone (see SI for further details). 18 structures possibly involved in this model reaction were calculated on the Ag(111) surface (also see Figure S17–S19 and following discussion). These structures range from the starting compounds (chosen as reference state with a relative energy of 0 kJ mol^{-1}, in Figure 6 referred to as Ph-NH_2 + Ph-

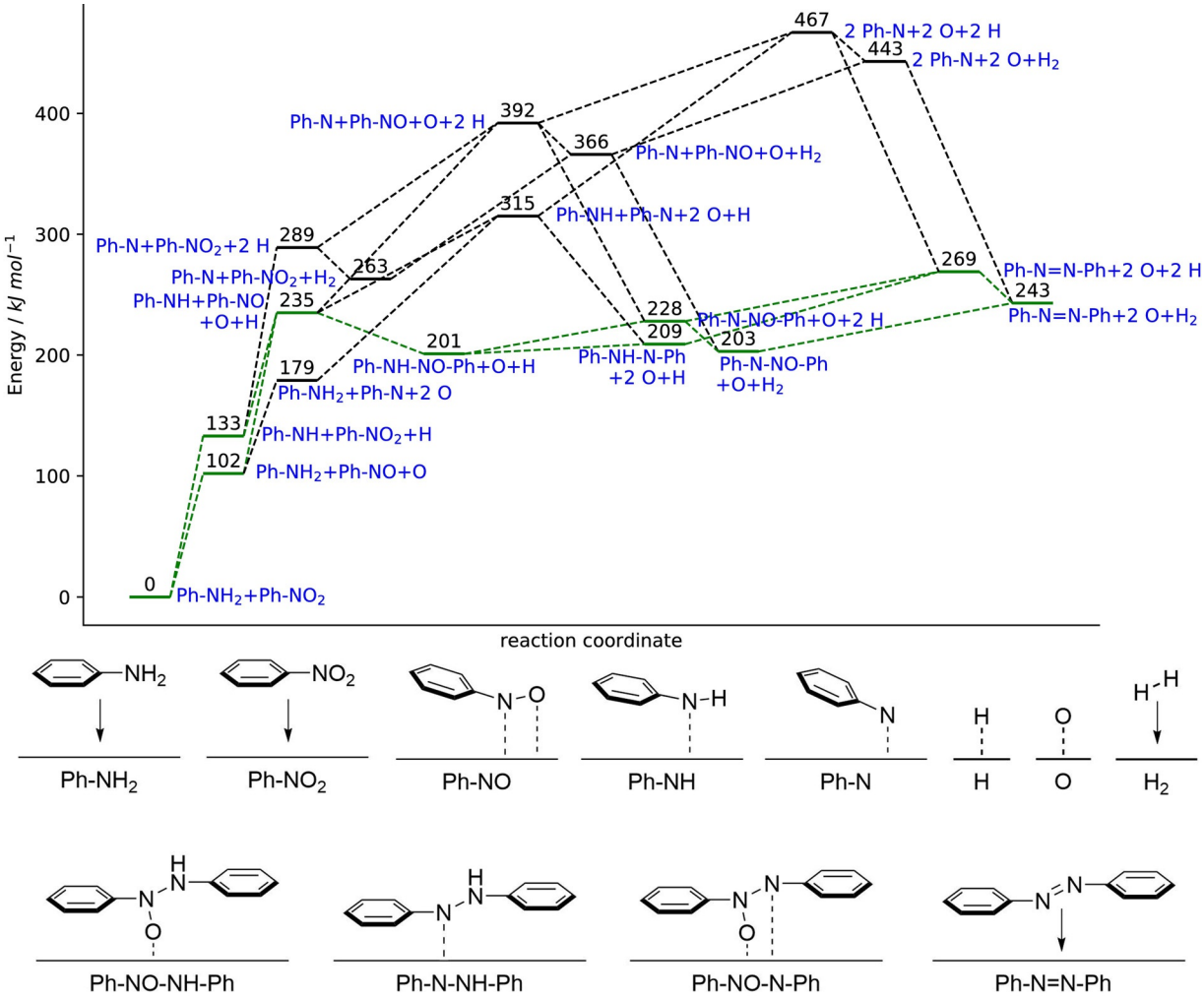

Figure 6. Calculated energy profile of the reaction of aniline and nitrobenzene on Ag(111) and corresponding structures. Two possible pathways via the most energetically favorable intermediate structures are highlighted in green color. All alternative routes are shown as dashed black lines.

NO_2) to *trans*-azobenzene (co-adsorbed with two oxygen atoms and one H_2 molecule, Ph−N=N−Ph + 2 O + H_2). The resulting energy profile can be seen in Figure 6. Please note that no reaction barriers or transition states were calculated (also see the discussion following Figure S19 for further details).[33] Two pathways connecting the intermediates with the lowest energies are highlighted in green color. As first steps, an H atom and an O atom are removed from aniline and nitrobenzene at the cost of approximately 133 kJ mol^{-1} and 102 kJ mol^{-1}, respectively. These two processes lead to the intermediate structure Ph−NH + Ph−NO + O + H, which is 235 kJ mol^{-1} higher in energy. Next, an N−N single bond can be formed, releasing approximately 34 kJ mol^{-1}. The intermediate Ph−NH−NO−Ph can then lose the nitrogen-bound H and O atoms in a slightly endothermic stepwise procedure to form the azo product. Since hydrogen atoms form H_2 with a very low reaction barrier of < 25 kJ mol^{-1}[34] on Ag(111), it can be expected that the two abstracted H atoms can recombine at any time during the reaction, which presumably suppresses the formation of other by-products apart from H_2 and adsorbed O atoms. This recombination is exothermic by approximately 25 kJ mol^{-1}. Considering that the reactions are performed under UHV conditions and that the adsorption energy of H_2 molecules on Ag(111) surfaces is very small (< 10 kJ mol^{-1}), it can be assumed that newly formed H_2 molecules will be quickly and continuously removed from the equilibrium. Naturally, this enhances the formation of H_2 and will contribute to the driving force of the overall endothermic on-surface reaction. The gain in entropy resulting from the desorption of H_2 has been identified as driving force in other on-surface reactions,[35,36] further supporting the formation and desorption of H_2. Contrary to hydrogen, the abstracted oxygen atoms are observed to remain—at least partially—adsorbed on the surface, even at elevated temperatures (Figure S14). This agrees well with literature, where the recombinative desorption of O_2 on the Ag(111) surface is observed at temperatures higher than 597 K.[37]

Conclusion

In summary, on-surface azo group formation was realized on silver surfaces. STM results reveal that the azo group formation by nitro–amino redox cross-coupling (path **1**) is the most efficient reaction on the silver surface in comparison with nitro–nitro (path **2**) and amino–amino homocoupling (path **3**). XPS measurements, as well as theoretically and experimentally analyzed model compounds further supported the correct structural assignment after reaction on silver surface. Using well-designed molecular precursors, azo polymers were successfully prepared. Experiments at different surfaces revealed that the metal types and the surface structures have a significant influence on the reaction outcome. A mechanistic model was developed based on the XPS study and dimerization reactions of possible intermediates as model compounds. Based on a DFT study a stepwise splitting of N−H and N−O bonds from the starting material along N−N bond formation was suggested as the most likely reaction path. Our work provides a new bottom-up strategy to synthesize functional materials through on-surface reactions.

Acknowledgements

We thank the Deutsche Forschungsgemeinschaft (SFB 858, TRR 61, FU 299/19, GA2430/1-1, MO 2345/4-1, and AM 460/2-1) for financial support. H.-Y.G. acknowledges financial support by NSFC within Grant 21972104 and "1000-Youth Talents Plan". X.M. thanks the Alexander von Humboldt foundation for financial support. H.K. wants to thank Dr. Anup Bhunia and Niklas Radhoff for helpful discussions. Open access funding enabled and organized by Projekt DEAL.

Conflict of interest

The authors declare no conflict of interest.

Keywords: Azo formation · conjugated polymers · cross-coupling · STM · surface chemistry

[1] Q. Shen, H. Y. Gao, H. Fuchs, *Nano Today* **2017**, *13*, 77 – 96.
[2] P. A. Held, H. Fuchs, A. Studer, *Chem. Eur. J.* **2017**, *23*, 5874 – 5892.
[3] T. Wang, J. Zhu, *Surf. Sci. Rep.* **2019**, *74*, 97 – 140.
[4] S. Clair, D. G. de Oteyza, *Chem. Rev.* **2019**, *119*, 4717 – 4776.
[5] S. Weigelt, C. Busse, C. Bombis, M. M. Knudsen, K. V. Gothelf, T. Strunskus, C. Wöll, M. Dahlbom, B. Hammer, E. Lægsgaard, F. Besenbacher, T. R. Linderoth, *Angew. Chem. Int. Ed.* **2007**, *46*, 9227 – 9230; *Angew. Chem.* **2007**, *119*, 9387 – 9390.
[6] S. Weigelt, C. Busse, C. Bombis, M. M. Knudsen, K. V. Gothelf, E. Lægsgaard, F. Besenbacher, T. R. Linderoth, *Angew. Chem. Int. Ed.* **2008**, *47*, 4406 – 4410; *Angew. Chem.* **2008**, *120*, 4478 – 4482.
[7] L. Jiang, A. C. Papageorgiou, S. C. Oh, Ö. Sağlam, J. Reichert, D. A. Duncan, Y. Q. Zhang, F. Klappenberger, Y. Guo, F. Allegretti, S. More, R. Bhosale, A. Mateo-Alonso, J. V. Barth, *ACS Nano* **2016**, *10*, 1033 – 1041.
[8] M. Treier, N. V. Richardson, R. Fasel, *J. Am. Chem. Soc.* **2008**, *130*, 14054 – 14055.
[9] N. Ruiz del Árbol, I. Palacio, G. Otero-Irurueta, J. I. Martínez, P. L. de Andrés, O. Stetsovych, M. Moro-Lagares, P. Mutombo, M. Svec, P. Jelínek, A. Cossaro, L. Floreano, G. J. Ellis, M. F. López, J. A. Martín-Gago, *Angew. Chem. Int. Ed.* **2018**, *57*, 8582 – 8586; *Angew. Chem.* **2018**, *130*, 8718 – 8722.
[10] A. Basagni, L. Colazzo, F. Sedona, M. Di Marino, T. Carofiglio, E. Lubian, D. Forrer, A. Vittadini, M. Casarin, A. Verdini, A. Cossaro, L. Floreano, M. Sambi, *Chem. Eur. J.* **2014**, *20*, 14296 – 14304.
[11] S. Boz, M. Stöhr, U. Soydaner, M. Mayor, *Angew. Chem. Int. Ed.* **2009**, *48*, 3179 – 3183; *Angew. Chem.* **2009**, *121*, 3225 – 3229.
[12] F. Bebensee, C. Bombis, S. R. Vadapoo, J. R. Cramer, F. Besenbacher, K. V. Gothelf, T. R. Linderoth, *J. Am. Chem. Soc.* **2013**, *135*, 2136 – 2139.
[13] O. Díaz Arado, H. Mönig, H. Wagner, J. H. Franke, G. Langewisch, P. A. Held, A. Studer, H. Fuchs, *ACS Nano* **2013**, *7*, 8509 – 8515.
[14] S. Jaekel, A. Richter, R. Lindner, R. Bechstein, C. Nacci, S. Hecht, A. Kühnle, L. Grill, *ACS Nano* **2018**, *12*, 1821 – 1828.

[15] L. Q. Zheng, X. Wang, F. Shao, M. Hegner, R. Zenobi, *Angew. Chem. Int. Ed.* **2018**, *57*, 1025 – 1029; *Angew. Chem.* **2018**, *130*, 1037 – 1041.
[16] C. Nacci, M. Baroncini, A. Credi, L. Grill, *Angew. Chem. Int. Ed.* **2018**, *57*, 15034 – 15039; *Angew. Chem.* **2018**, *130*, 15254 – 15259.
[17] P. Tomkins, E. Gebauer-Henke, W. Leitner, T. E. Müller, *ACS Catal.* **2015**, *5*, 203 – 209.
[18] Q. Li, B. Yang, J. Björk, Q. Zhong, H. Ju, J. Zhang, N. Cao, Z. Shi, H. Zhang, D. Ebeling, A. Schirmeisen, J. Zhu, L. Chi, *J. Am. Chem. Soc.* **2018**, *140*, 6076 – 6082.
[19] M. Knor, H. Y. Gao, S. Amirjalayer, A. Studer, H. Gao, S. Du, H. Fuchs, *Chem. Commun.* **2015**, *51*, 10854 – 10857.
[20] P. Iqbal, K. Critchley, D. Attwood, D. Tunnicliffe, S. D. Evans, J. A. Preece, *Langmuir* **2008**, *24*, 13969 – 13976.
[21] P. Mendes, M. Belloni, M. Ashworth, C. Hardy, K. Nikitin, D. Fitzmaurice, K. Critchley, S. Evans, J. Preece, *ChemPhysChem* **2003**, *4*, 884 – 889.
[22] L. Kankate, A. Turchanin, A. Gölzhäuser, *Langmuir* **2009**, *25*, 10435 – 10438.
[23] A. Mesnage, X. Lefèvre, P. Jégou, G. Deniau, S. Palacin, *Langmuir* **2012**, *28*, 11767 – 11778.
[24] M. Toupin, D. Bélanger, *J. Phys. Chem. C* **2007**, *111*, 5394 – 5401.
[25] Y. Xu, Z. Li, F. Zhang, X. Zhuang, Z. Zeng, J. Wei, *RSC Adv.* **2016**, *6*, 30048 – 30055.
[26] G. Iucci, G. Polzonetti, P. Altamura, G. Paolucci, A. Goldoni, R. D'Amato, M. V. Russo, *Appl. Surf. Sci.* **1999**, *153*, 10 – 18.
[27] Y. P. Lin, O. Ourdjini, L. Giovanelli, S. Clair, T. Faury, Y. Ksari, J. M. Themlin, L. Porte, M. Abel, *J. Phys. Chem. C* **2013**, *117*, 9895 – 9902.
[28] M. Matena, J. Björk, M. Wahl, T. L. Lee, J. Zegenhagen, L. H. Gade, T. A. Jung, M. Persson, M. Stöhr, *Phys. Rev. B* **2014**, *90*, 125408.
[29] L. Sharma, T. Matsuoka, T. Kimura, H. Matsuda, *Polym. Adv. Technol.* **2002**, *13*, 481 – 486.
[30] A. Adenier, E. Cabet-Deliry, A. Chaussé, S. Griveau, F. Mercier, J. Pinson, C. Vautrin-Ul, *Chem. Mater.* **2005**, *17*, 491 – 501.
[31] J. Perdew, K. Burke, M. Ernzerhof, *Phys. Rev. Lett.* **1996**, *77*, 3865 – 3868.
[32] J. Perdew, K. Burke, M. Ernzerhof, *Phys. Rev. Lett.* **1997**, *78*, 1396.
[33] Such calculations are out of reach with our present resources within a reasonable time frame. Formally, our discussion relies on the somewhat drastical assumption that the Hammond's postulate[38] linking product stability and barrier height is applicable for on-surface reactions. For further information, see discussion continuing Figure S19.
[34] X.-L. Zhou, J. M. White, B. E. Koel, *Surf. Sci.* **1989**, *218*, 201 – 210.
[35] "Kinetic and thermodynamic considerations in on-surface synthesis": J. Björk in *On-surface synthesis II* (Eds.: D. G. de Oteyza, C. Rogero), Springer, Heidelberg, **2018**, pp. 19 – 34.
[36] K. L. Svane, B. Hammer, *J. Chem. Phys.* **2014**, *141*, 174705.
[37] C. T. Campbell, *Surf. Sci.* **1985**, *157*, 43 – 60.
[38] G. S. Hammond, *J. Am. Chem. Soc.* **1955**, *77*, 334 – 338.

Manuscript received: August 31, 2020
Accepted manuscript online: November 16, 2020
Version of record online: December 11, 2020

